Pore Structure and Its Controls of Shale in the Qingshankou Formation, Sanzhao Sag, Songliao Basin

Surong Zhang [1], Songtao Wu [2,*], Rukai Zhu [1], Jingya Zhang [1], Chang Liu [1], Tianshu Zhang [1], Yi Cai [1], Mengying Li [1], Ganlin Hua [3], Yuan Kang [4] and Bo Wang [4]

1   Research Institute of Petroleum Exploration and Development (RIPED), China National Petroleum Corporation (CNPC), Beijing 100083, China; zsr_win2019@163.com (S.Z.)
2   National Energy Tight Oil and Gas R&D Center, Beijing 100083, China
3   School of Energy Resources, China University of Geosciences, Beijing 100083, China
4   Institute of Energy, School of Earth and Space Sciences, Peking University, Beijing 100871, China
*   Correspondence: wust@petrochina.com.cn; Tel.: +86-150-1146-0695

Abstract: The exploration and development of Gulong shale oil in the Songliao Basin has achieved a major breakthrough, with the result that a national shale oil demonstration area is being built. The shale in the Sanzhao Sag is abundant in organic matter and is an important replacement area. For this reason, it has recently become a focus for research and exploration. Compared with the Gulong Sag, the Qingshankou Formation in the Sanzhao Sag is relatively immature, and comparatively little is known about its pore structure. For this study, well ZY1, a key well in the Sanzhao Sag, was selected as the research object. Thin section observation, high-resolution field emission scanning electron microscopy, Modular Automated Processing Systemimaging, X-ray diffraction of whole rock and clay, TOC pyrolysis, and Low-pressure N_2 adsorption were used to investigate the pore structure in the sag to determine the factors influencing pore development. The principal understandings are as follows: (1) The Qingshankou Formation in the Sanzhao Sag is predominantly clay shale, with a high content of clay minerals (32.8 to 70%) and TOC contents of 0.7 to 11%. These values indicate good hydrocarbon generation potential. (2) Interparticle pores, intraparticle pores, and organic matter pores are developed. Intergranular pores are the main type, mostly observed between granular minerals or between granular minerals and clays. Intraparticle pores are observed in pyrite mass and dissolved unstable minerals. Organic matter pores (OMP) occur in primary organic matter and migrate into solid bitumen. (3) The shale pores in the Sanzhao Sag are mainly H3-type slit pores, with specific surface areas of 5.4~22.9 m^2/g and pore volumes of 0.03~0.07 cm^3/g. Mesopores make the largest contribution to pore volume and specific surface area. Scanning electron microscope (MAPS) imaging shows that the pore size distribution of shale is mainly 20~30 nm and 100~200 nm and that large pores, especially pores of 100~200 nm and 1~2 μm, make the largest contribution to the facies. (4) The pore structure in the Sanzhao Sag is affected by mineral composition, abundance of organic matter, thermal evolution degree, and diagenesis. Organic-inorganic interactions influence and determine the pore structure characteristics of the Qingshankou Formation shale. This paper is intended to provide scientific guidance and technical support for evaluating the effectiveness of shale oil reservoirs and selecting sweet spots in the Sanzhao Sag.

Keywords: unconventional oil and gas; Gulong shale oil; Sanzhao sag; Qingshankou Formation; pore structure

1. Introduction

Reservoir quality is an important element in shale oil and gas research and has therefore long attracted the attention of geologists and explorers [1–4]. Accurate understanding of the pore structures of shale reservoirs at the micro- and nano-scales is a hot topic in research [5–9]. Key parameters such as size distribution, specific surface area, and volume

of shale pores can be quantitatively evaluated using experimental techniques such as gas adsorption, nuclear magnetic resonance (NMR), and high pressure mercury compression (HPMC) [10–16]. Under SEM, the pore type, pore space size, and morphological characteristics of shales can be directly observed [17–19], a method used in many studies for pore classification and analysis of the structural characteristics of different types of pores [20]. This combination of qualitative observation and quantitative analysis helps to explain the formation mechanisms of shale pores and thus improve understanding of the controlling factors of different types of pore structures.

Variations in mineral compositions and organic matter characteristics (type, content, and degree of evolution) are the main reasons for differences in shale storage capacity. Changes in mineral composition and lithology control the mechanical properties and pore structures of shale, thus controlling the increase and decrease in shale pore space [21]. The correlations between brittle minerals and pore space at various levels are related to different geological conditions and diageneses, which do not have a predictable pattern. Clay minerals are important components in mud shales, and the micro- and nano-pores associated with them are important inorganic pores in shale reservoirs. Microporosity is generally considered to be most developed in smectite, followed by an illite/smectite mixed layer, while pores developed in kaolinite are generally medium to large in size (20 nm~100 nm). There are fewer nanopores in chlorite and illite minerals [22]. The factors controlling pore structure are studied by analyzing the relationship between TOC contents and the thermal maturity of organic matter in shale. TOC content is positively correlated with pore volume, specific surface area, and porosity at all levels of pore space [23,24]. However, some studies have found that the positive correlation is not absolute. When TOC content exceeds a certain value, its correlations with pore volume and specific surface area are negligible or even negative [25,26]. Storage capacity evolves as a result of the thermal decomposition of organic matter during maturation. The degree of thermal evolution determines the pore type, pore volume, specific surface area, and particularly the pore structures of organic matter pores. Many studies have compared the pore characteristics of natural samples with different maturity levels or different artificial ripening stages of the same sample and have found that the correlation between organic matter maturity and organic matter pores is not positive [27–29]. Organic pores still develop in the immature stage. They are related to primary organic matter and inherit its original pore structure. In the mature stage, organic matter pores associated with hydrocarbon generation gradually increase, but at the peak of oil maturity (Ro = 0.85% to 1.2%), organic matter pores are less developed as solid bitumen fills and covers the pores [30–32]. At higher maturity, the pores in the shale that have been covered are released, and organic pores again appear in large numbers. The formation and evolution of shale pore systems is a complicated process involving interactions between inorganic minerals and organic matter. Different mineral compositions and organic matter characteristics determine the pore structures and controlling factors of different types of shale.

There has been a significant breakthrough in the Gulong shale oil in the Songliao Basin, with its main producing layer, the Qingshankou Formation shale, benefitting from high clay mineral content and high maturity. Clay mineral-related pores and organic pores are the main types in the Gulong shale. By comparing the pore structure characteristics of natural shale samples with different maturities in the Songliao Basin, Bo Liu found that the peak diameter of organic matter pores increased from 25 to 75 nm in samples with relatively low maturity (Ro < 0.95%). Pore sizes increased with an increase in maturity, and the diameter of inorganic matter pores gradually decreased. This confirmed that there are differences in pore structure between shales with different TOC contents at different stages of maturity [28].

The Sanzhao sag is a potentially important area for shale oil in the Songliao Basin. It has similar hydrocarbon generation conditions to the Gulong Sag, but lower maturity and higher TOC content. Studying the pore structure characteristics and analyzing the influencing factors of the pore structure of the sag will provide a more comprehensive

understanding of the pore structures of shale in different thermal evolution stages in the Songliao Basin as a whole. In this paper, shale samples from the Qingshankou Formation in the Sanzhao sag of the Songliao Basin were studied and their structural characteristics analyzed using thin section observation, XRF elemental scanning analysis, X-ray diffraction (XRD), quantitative evaluation using LPNA, qualitative observation using field emission scanning electron microscopy (FE-SEM) of argon ion polished samples, and qualitative classification and analysis using Modular Automated Processing System (MAPS) imagery. The controlling factors of pore structure in the Sanzhao sag are described in terms of mineral composition, TOC content, thermal evolution, and diagenesis, providing fundamental information to guide the selection of shale oil sweet spots with different maturity levels.

2. Geological Setting

The Songliao Basin, in northeastern China, is a large continental oil- and gas-bearing basin deposited in the Mesozoic and Neozoic. The basement is Palaeozoic metamorphic rock and igneous rock [33]. From bottom to top, the major formations are the Huoshiling Formation, the Shahezi Formation, the Yingcheng Formation, the Denglouku Formation, the Quantou Formation, the Qingshankou Formation, the Yaojia Formation, the Nenjiang Formation, the Sifangtai Formation, and the Mingshui Formation. The Qingshankou Formation was deposited during the Early Cretaceous, in a thermal subsidence depression stage during which hydrocarbon source rocks formed. In the late Cretaceous, contraction of the lake basin and differential uplift in the east shifted the sedimentary center westward, and regional extrusion caused an obvious tectonic inversion in the basin [34]. This inversion and differential subsidence led to different sedimentation and paleothermal flow rates, with the result that the degrees of thermal evolution of the shales of the Qingshankou Formation differ between the six sedimentary tectonic units of the Songliao Basin (the Central Depression, the Northern Dump, the Northeast Uplift, the Southeast Uplift, the Southwest Uplift, and the Western Slope) [35–37]. Vitrinite reflectance in the western part of the central depression is generally greater than 1%, in the central uplift it is about 0.75%, and in the eastern depression it is about 0.95%. The western slope and southeast uplift in this area were effectively obliterated around 72.5 Ma. Due to this uplift and denudation, the formation has not become mature, with vitrinite reflectance less than 0.5%, indicating immature organic matter.

The Sanzhao sag (including Zhaozhou, Zhaoyuan, and Zhaodong counties) is located in the central depressional zone in the northern part of the Songliao Basin, adjacent to Daqing Changyuan in the west and to the Chaoyanggou terrace in the east (Figure 1). In the north, it abuts the Suihua depression, the Suiling back-slope belt, and the southern part of the Anda vector. It is a long-term inherited developmental depression [38]. The Qingshankou Formation provides the source rocks for the Sanzhao Depression, which are somewhat undercompacted and overpressured at present due to their great thickness and rapid deposition rate. The Sanzhao area is a relatively low and gentle triangular depression. Strike-slip action along the boundary fractures has slowed the influence of tectonic stress on the interior of the depression, so the internal tectonic environment is stable. The organic matter thermal evolution history shows that the vitrinite reflectance of the Qingshankou Formation shale is 0.50–0.67% in the strata marking the end of the deposition of the Sifangtai Formation, 0.71–0.84% in the strata from the end of the deposition of the Mingshui Formation, and mostly 0.75–1.0% at the end of Neoproterozoic deposition. The source rock is mature [39]. Generally, high overpressure, a stable internal environment, and relatively low thermal evolution are the keys to the high reservoir quality of the shales in the Sanzhao sag.
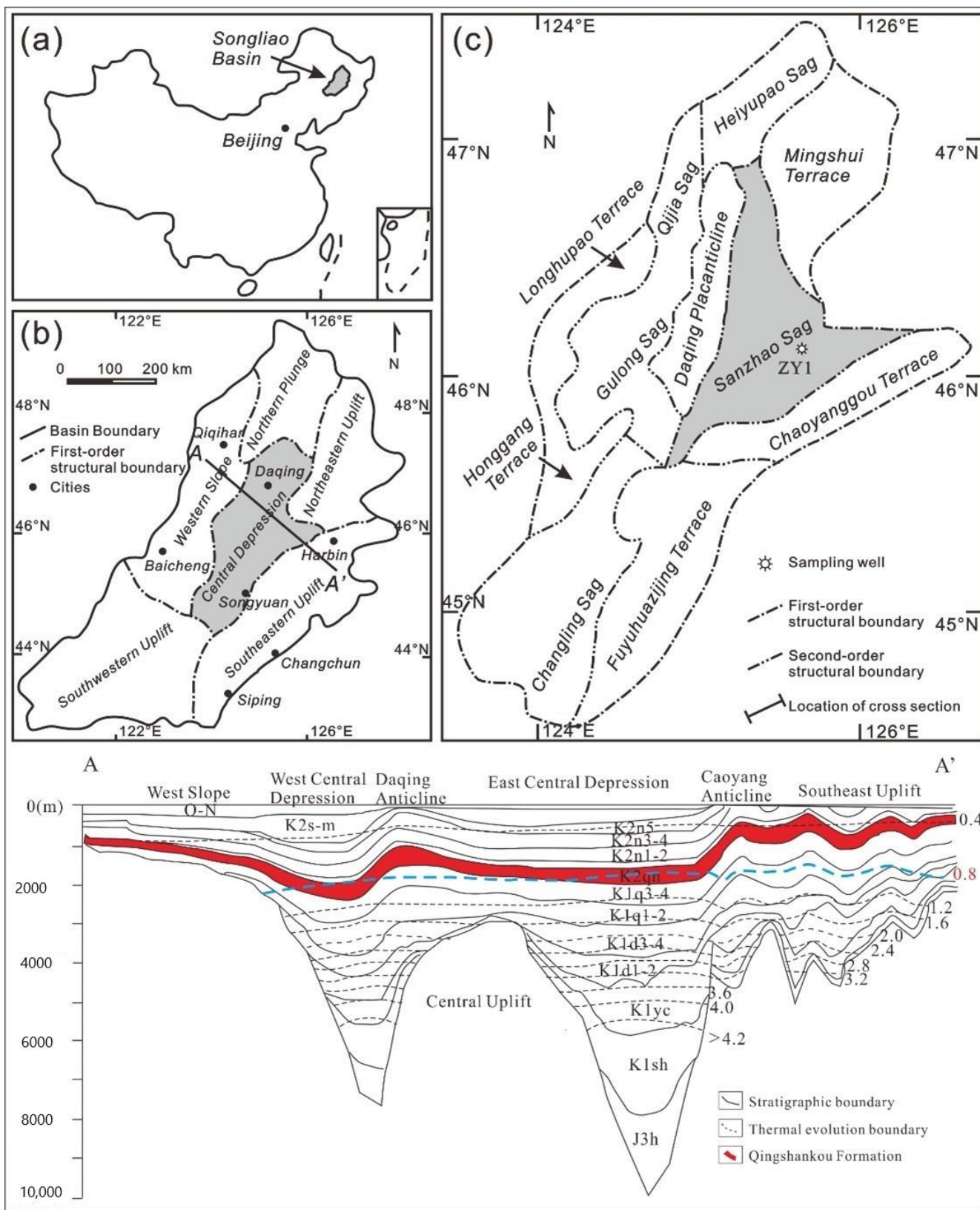
Figure 1. Regional geological map and cross section of Sanzhao sag in Songliao Basin (modified according to References [40,41]. (**a**) the location of songliao basin in China; (**b**) different structural units of Songliao Basin; (**c**) the location of Sanzhao Sag in Central Depression.

3. Samples and Methods

3.1. Samples

For this study, 18 samples were taken from shale cores from Well ZY1 in the first member of the Qingshankou Formation. Deposition of this member occurred in a reductive, deep lacustrine environment. The lithology is mainly black-gray clay shale, and the sedimentary structure is massive and homogeneous, with few or no laminae developed. The samples were analyzed using thin sections, FE-SEM, energy spectrum (ES), Qemscan, TOC content, pyrolysis, and low-pressure N_2 adsorption (LPNA) in order to determine the pore development characteristics of the middle and low maturity shale and analyze the factors controlling their pore structures in comparison with the high maturity Gulong shales.

3.2. Thin Section and SEM Observation

A LEICA polarizing microscope was used to carry out multi-purpose observations on polished, double-sided thin slices. Images can be obtained on this instrument using single or orthogonal polarization modes with magnifications between 20 and 400 times to qualitatively determine the lithology, mineral composition, and grain layer characteristics of the sample. Samples for FE-SEM observation under a field emission scanning electron microscope were ion-polished. The samples were cut into relatively flat $1 \times 1 \times 2$ mm squares and manually polished with 800 mesh, 1000 mesh, and 2000 mesh sandpaper, respectively. A Leica argon ion polishing instrument was used to polish the circumferences of the samples to ensure smooth surfaces before carbon plating. SEM observation was performed using an FEI Apreo high-resolution FE-SEM at a working voltage of 2 kV and a working distance of 4.0 mm. Scanning electron microscopy was used for high-resolution imaging to observe mineral morphology, occurrence, dissolution, and pore characteristics.

3.3. MAPS

MAPS images were acquired using the Apreo high-resolution FE-SEM with an operating voltage of 5 kV, operating current of 0.4 nA, an operating distance of 4.0 mm, and a single image pixel point resolution of 10 nm, with 750 photographs being acquired for each sample. Avizo9 image processing software was used to stitch the images together, and the watershed method was used for pore identification. Parameters such as pore diameter and specific surface area were calculated using an equivalent circle model.

3.4. XRD

X-ray diffraction (XRD) analysis was performed using a TTR-type X-ray diffractometer manufactured by Rigaku, Japan. Samples were pre-processed by crushing to a 200 mesh powder. The experiment was carried out according to the standard "X-ray diffraction Analysis Method for Clay Minerals and Ordinary Non-clay Minerals in Sedimentary Rocks", with an error of less than 10%.

3.5. Total Organic Carbon (TOC) Determination and Rock-Eval Pyrolysis

For Pyrolysis and TOC calculation, the core block samples were crushed to 200 mesh powder. Pyrolysis was performed under normal temperature and pressure using a ROCK-EVAL6 pyrolyzer. Organic carbon analysis was performed according to GB/T 19145-2003 using a LECO CS-230 carbon and sulfur analyzer at a constant temperature of 300 °C for 3 min for S_1 and a programmed temperature increase in 25 °C/min from 300 to 800 °C for S_2.

3.6. LPNA

Low-pressure N_2 adsorption-desorption measurements were performed with a Micromeritics ASAP2460 surface area and pore size analyzer. Samples were first ground to 60~80 mesh powder and then automatically degassed in a vacuum for over 8 h at 105 °C. This removed adsorbed moisture and volatile matter. N_2 adsorption-desorption isotherms were obtained at −197 °C under relative pressures (P/P0) of 0.01 to 0.995. The equilibrium time for

adsorption and desorption at each pressure point was 15 s. The pore size distribution and total pore volume were determined based on the Density Functional Theory (DFT) model.

3.7. QEMSCAN

QEMSCAN mineral analysis was performed using an FEI Quanta 450 field emission scanning electron microscope with an operating voltage of 15 kV, an electron beam current of 0.8 nA, a spacing of 1.5 μm/point for energy spectroscopy, and a scanning range of 3 mm × 3 mm. This technique allows detailed characterization of the compositions, contents, grain sizes, and contact relationships of minerals in dense sandstones.

The experiments were carried out at the Geology Experimental Research Center of the Research Institute of Petroleum Exploration and Development, except for the nitrogen adsorption experiments, which were carried out at the Institute of Unconventional Oil and Gas of Northeast Petroleum University.

4. Results

4.1. Shale Composition

The organic matter type in the shale of the Qingshankou Formation is I-II$_1$. The TOC content is high, 0.7~11%, with an average of 4%. Free hydrocarbon content (S1) is 0.2 mg/g~5.2 mg/g, increasing with an increase in TOC content. HI is stable at 500 mg/g. When TOC > 2%, HI tends to be stable, reflecting a homogenous source contribution. An intersection diagram of TOC content and hydrocarbon generation potential (TOC-S1+S2) shows that the shale of the first member of the Qingshankou Formation in Well ZY1 is excellent hydrocarbon source rock (Figure 2).
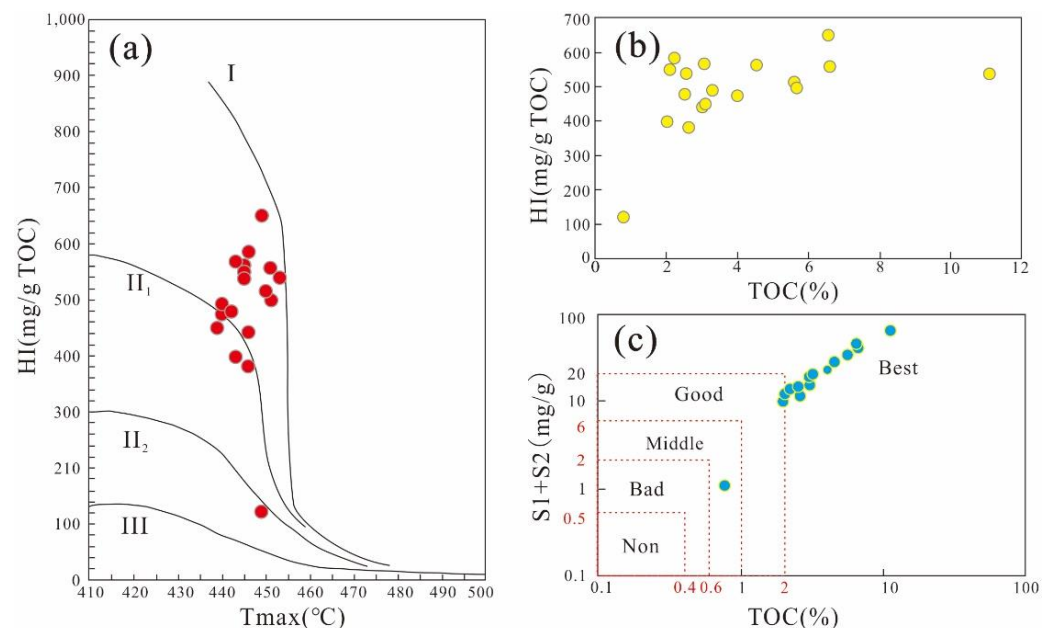

Figure 2. Geochemical characteristics and hydrocarbon generation potential of the first member of Qingshankou Formation in Sanzhao Sag. (**a**) Kerogen type, mainly I-II$_1$; (**b**) Relationship between TOC and HI, HI is stable at 500 mg/g. When TOC > 2%, HI tends to be stable. (**c**) (TOC-S1+S2) shows different levels of source rock, shales in in Well ZY1 is excellent hydrocarbon source rock.

XRD analysis shows that the composition of the shale in the section of the Qingshankou Formation in the Sanzhao area is predominantly clay minerals (32.8~70%/53.1%) and quartz (18.6~33.11%/24.9%), followed by plagioclase (3.6~18.8%/8.9%), and small amounts of iron dolomite, calcite, and pyrite. The clay mineral composition is high in the illite/smectite mixed layer (26~63%/46.2%), followed by illite (19~66%/34.2%), with small amounts of chlorite and the chlorite/smectite mixed layer (Table 1).

Table 1. Geochemical characteristics and XRD characteristics of shale in the first member of Qingshankou Formation of ZY1.

| No. | Burial Depth, m | Rock-Eval | | | | | | | Whole-Rock Mineralogy, wt.% | | | | | | | Clay (Phyllosilicate) Mineralogy, wt.% | | | |
		TOC, wt.%	Tmax, °C	S_1, mg/g	S_2, mg/g	S_3, mg/g	HI (mg/g. TOC)	Quartz	Plagioclase	Calcite	(Fe-) Dolomite	Siderite	Pyrite	Total Clay	Illite	Chlorite	Illite/ Smectite	Chlorite/ Smectite
1	1982	2.49	442	2.3	11.9	0.2	477	30	18.8	10	0	0	4.6	36.2	34	22	44	0
2	1996	4.51	445	3.1	25.4	0.2	563	21.9	9.6	2.1	8.2	0.0	3.1	55.0	48.	9.0	38.0	5.0
3	2000	3.03	443	1.5	17.2	0.3	567	21.4	9.4	7.8	0	3	3.8	54.5	40	3	55	2
4	2005	2.06	445	0.9	11.3	0.2	550	22.2	8.5	0.0	0.0	0.0	3.1	66.2	66.	6.0	26.0	2.0
5	2008	3.08	439	1.6	13.9	0.3	450	19.9	6.4	0.0	0.0	0.0	3.7	70.0	34.	10.0	53.0	3.0
6	2013	2.21	446	1.1	12.9	0.3	584	19.9	8.2	0.0	16.4	0.0	5.9	49.6	48.	11.0	38.0	3.0
7	2016	6.54	449	2.9	42.5	0.2	649	28.6	13.6	0.0	0.0	0.0	0.0	57.8	23	20	49	8.0
8	2021	2.59	446	1.9	9.9	0.6	381	24.1	6.9	0.0	19.4	3.6	3.7	42.3	19.	19.0	54.	8.0
9	2023	2.99	446	2.5	13.2	0.3	442	19.8	8.1	0.0	16.4	0.0	4.1	51.6	43	11	42	4.0
10	2026	6.58	451	4.3	36.7	0.2	557	25.1	13.3	0.0	0.0	1.9	4.4	55.3	21	19	53	7.0
11	2031	5.58	450	5.2	28.7	0.2	515	26.5	8.8	0.0	0.0	2.4	3.2	59.2	47	17	28	8.0
12	2036	11.0	453	4.8	59.7	0.2	538	28.6	13.5	0.0	0.0	0	0	57.9	21	14	60	5.0
13	2041	3.98	440	4.3	18.8	0.3	473	18.6	3.6	6.0	0.0	36.2	2.7	32.8	19	11	63	7.0
14	2042	3.28	440	4.1	16.1	0.3	490	28.3	5.3	3.2	0.0	0.0	3.6	59.6	26	12	58	4.0
15	2046	5.66	451	4.9	28.2	0.3	499	33.1	6.2	0.0	0.0	0.0	3.6	57.1	38	18	33	11.0
16	2049	1.99	443	2.1	7.9	0.2	398	24.4	3.9	14	0.0	0.0	2.9	55.1	28	16	50	6.0
17	2052	0.77	449	0.2	0.9	0.3	122	30.9	7.4	20	0.0	0.0	0.0	42.1	26	20	42	12.0

4.2. Structural Characteristics

The 'sweet spots' of Chinese terrestrial shale reservoirs can be divided into three types: interbedded shale, mixed shale, and pure shale [42]. The "sweet spot" of oil accumulation in a continental shale source system refers to favorable reservoir distribution areas (intervals) that are relatively rich in oil, have better physical properties, are easier to transform, and have commercial development value under the current economic and technological conditions. In the context of the overall oil bearing, porosity, micro-fracture, and TOC are the important parameters. The Qingshankou Formation shale in the Songliao Basin represents a pure shale reservoir with effective pore space and adequate percolation capacity and is both an oil-generating and an oil-storing layer. Core description and thin section observation show that the shale facies in the section of the Qingshankou Formation in the Sanzhao Depression can be divided into three categories according to sedimentary structure: a generally homogeneous massive structure (Figure 3(A1–A3)), a millimeter-scale laminated structure (Figure 3(B1–B3)), and an easily fractured shale structure (Figure 3(C1–C3)). In the Sanzhao sag, the lithofacies are mainly massive shale (mudstone) or shale with faint laminae.
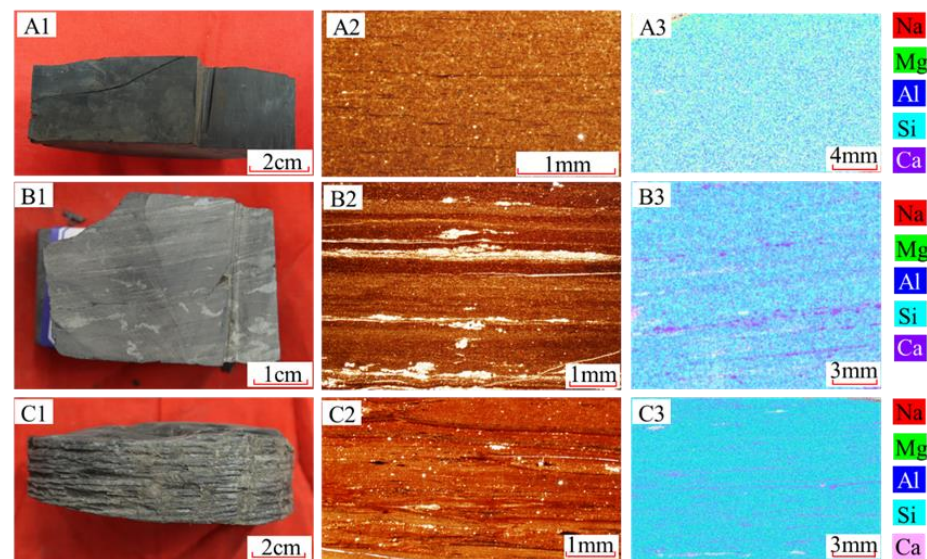
Figure 3. Lithofacies classification of shale in the first member of the Qingshankou Formation in ZY1well. (**A1**) Massive black shale, observed in core samples, with no laminae, 2031.1 m; (**A2,A3**) Massive gray-black shale, observed using thin section and XRF with no laminae 2021.1 m; (**B1**) felsic laminated shale, with bioturbation structures, 1982.1 m; (**B2,B3**) felsic laminated shale, horizontal thinner laminae, 2041.1 m; (**C1**) lamellated shale, easily broken, 2001.1 m (149); (**C2,C3**) lamellated shale, with thin pyrite laminae, overly homogeneous, 1989.6 m.

4.3. Pore Types

The classification of shale pores set out in Loucks et al., 2012 divides shale pores into mineral granular pores, organic pores, and fractures. Mineral granular pores are further divided into interparticle pores and intraparticle pores [6].

4.3.1. Interparticle Pores

Interparticle pores (InterP pores) are remainder pores supported by the skeletons of mineral particles. Pore morphology is generally related to the arrangement of mineral particles, and the pores are mostly narrow or irregularly polygonal. The pore sizes of intergranular pores are mainly 90 m~200 nm, with some macropores larger than 5 μm. The intergranular pores in the Qingshankou Formation shale in the Sanzhao area can be divided into three categories: (1) Pores (fractures) between clay minerals and mineral particles, which are mostly in the shape of narrow sutures under compaction (Figure 4A); (2) Pores between particles, distributed along and between mineral particles, with morphology controlled by the distribution of mineral particles (Figure 4B–H). The pores are mostly cemented by authigenic minerals such as chlorite, quartz, pyrite, etc. Authigenic minerals such as chlorite, quartz, and pyrite developed in the intergranular pores, and the residual intergranular pores were filled with migrated solid bitumen. The growth of authigenic minerals here is earlier than that of migrated solid bitumen, because authigenic quartz and chlorite have perfect crystalline forms (Figure 4C,D,H), and there are traces of dissolution in the edges of authigenic minerals (Figure 4D,F); (3) Pores between clay platelets, distributed along the clay minerals (illite or illite/smectite mixed layer), form multi-layer parallel seams, between which authigenic minerals such as quartz, calcite, and other minerals occur. These seams are generally filled with organic matter (Figure 4I).
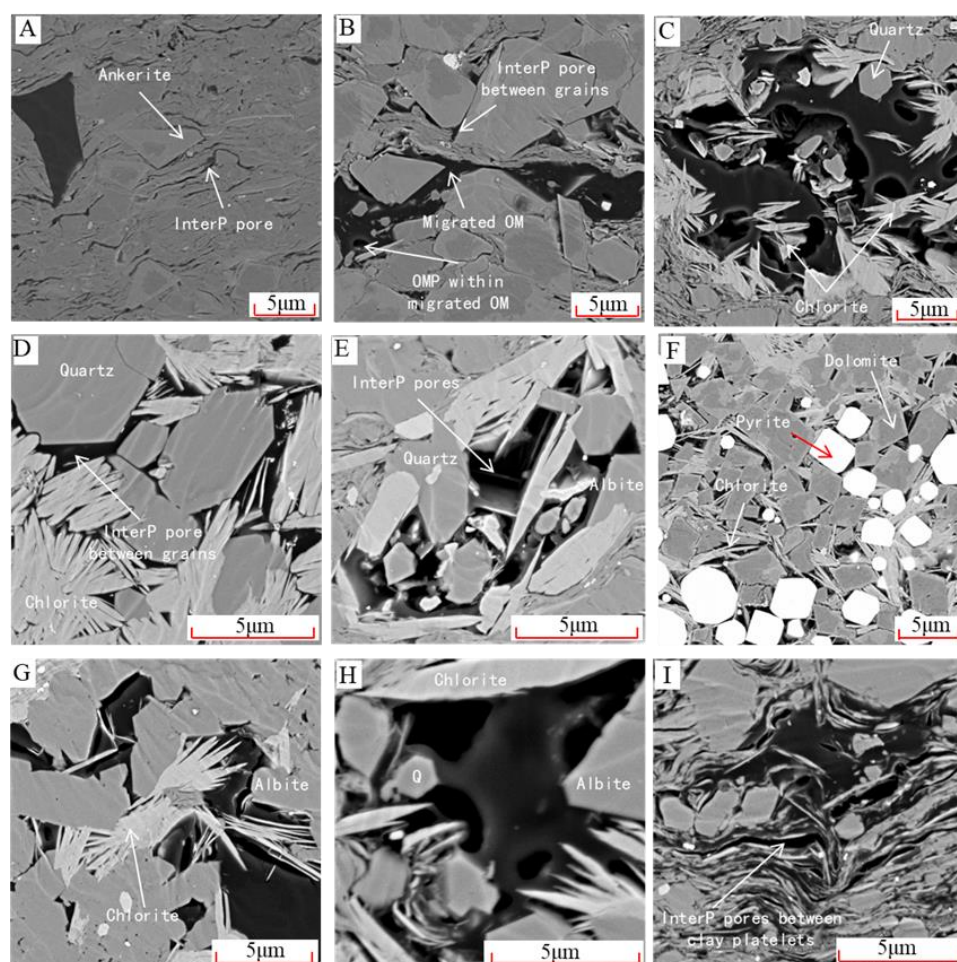
Figure 4. Interparticle pores. (**A**) Pores and fractures formed between mineral particles and clay minerals. The particles are mainly ankerite. (**B**) interparticle pores filled with a seam of migrating organic matter; (**C**) Authigenic chlorite, quartz, and other minerals support large interparticle pores, which are later filled with organic matter. (**D**), pores developed between rigid grains and chlorite, filled with OM. (**E**) pores bounded by quartz, chlorite, and feldspar; (**F**) Pores between ankerite and pyrite. They are in point contact but are filled with chlorite, reducing the pore volume; (**G**) Pores between grains, filled with organic matter and displaying organic matter shrinkage fractures, developed at the contact edges between organic matter and minerals. (**H**) Pores bounded by chlorite, quartz, and alacrite, filled with organic matter and developing micron-scale organic pores. (**I**) pores between clay platelets. The morphology of the pores and fractures are long seams controlled by the distribution of clay layers.

4.3.2. Intraparticle Pores

Intraparticle pores are pores within mineral particles or crystals, mostly in the form of dissolution intraparticle pores, but also occurring as cleavage-sheet intraparticle pores, fossil-cavity intraparticle pores, and intercrystalline intraparticle pores within pyrite framboids. The Qingshankou Formation shale contains many underdeveloped pores within pyrite framboids (Figure 5A). Most pyrite is aggregated in fossil cavities (Figure 5B) and in pores that have been filled with organic matter and oil (Figure 5C,D). Dissolution pores in the Sanzhao area are most commonly intraparticle pores. Most of them are dissolved pores within k-feldspar (Figure 5E–G), with a lesser amount of albite dissolution. Dissolution occurs mostly inside potassium feldspar grains (Figure 5E,F), forming dissolution intraparticle pores. Some dissolution also occurs at the edges of grains (Figure 5G), forming dissolution edge pores. FE-SEM showed that the dissolution pores are large, mostly 900~1000 nm, with the largest pore sizes up to 9 μm. These pores have good connectivity. The dissolved

pores are mostly filled with organic matter that may accelerate the dissolution of unstable minerals as a result of the organic acids produced by hydrocarbon generation from the organic matter. Intraparticle pores related to clay minerals are cleavage-sheet intraparticle pores, which are generally linear and parallel to one another within authigenic chlorite (Figure 5H,I). Fossil-cavity intraparticle pores form within the bodies of fossils that were dissolved with the resulting voids becoming filled with pyrite and organic matter. The shells are replaced by calcite, which then defines the boundaries of the pores (Figure 5B). These fossil cavities are particularly rich in organic matter, which can decompose into oil that encases pyrite (Figure 5D).
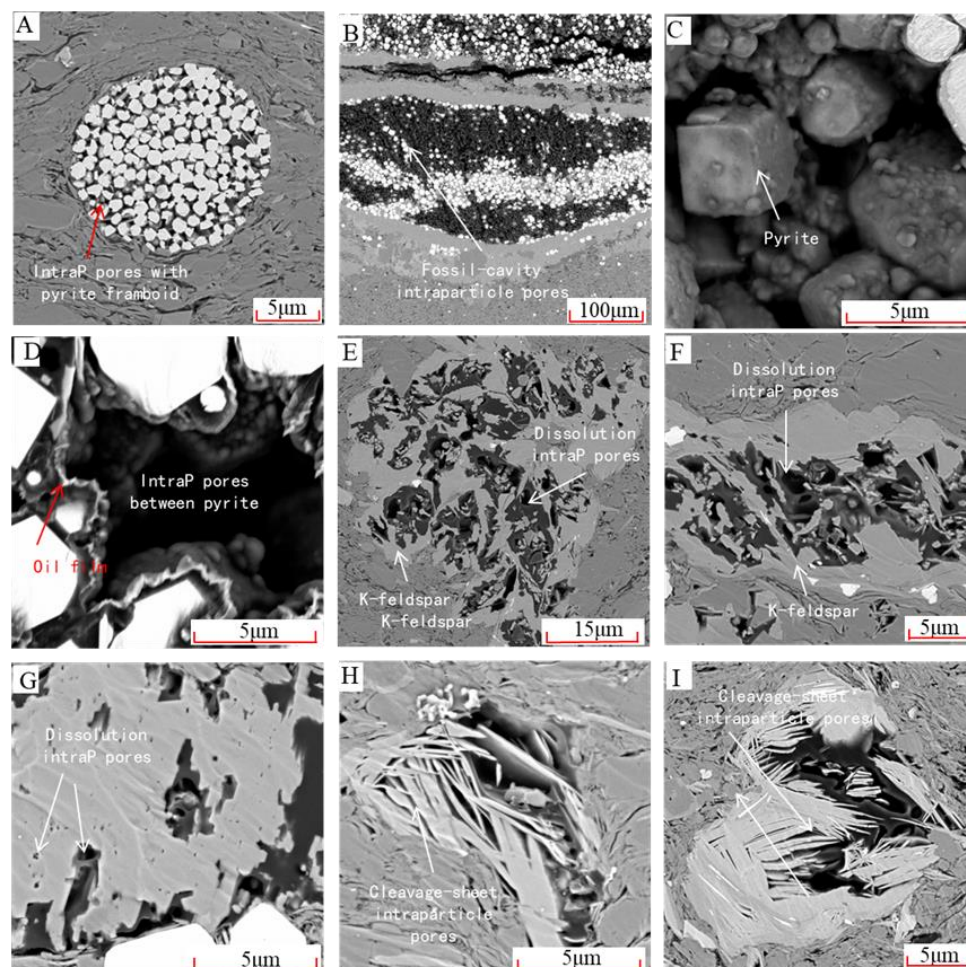

Figure 5. Intraparticle pores. (**A**) Intercrystalline intraparticle pores within a pyrite framboid. (**B**) Fossil-cavity intraparticle pores between pyrites, defined by fossil shells; (**C**) Pores in the pyrite body. The surface of the pyrite is polluted by organic matter; (**D**) Organic matter covers and wraps pyrite crystals in the form of oil fill. (**E–G**) Dissolution pores in k-feldspar grains connected and filled with organic matter. (**H,I**) Cleavage-sheet intraparticle pores, which are linear and delimited by authigenic chlorite. The pores in I are filled with organic matter.

4.3.3. Organic Matter Pores

Organic matter pores are pores within organic matter. The development of organic matter pores in the Sanzhao area is related to the structure of primary organic matter and to hydrocarbon generation. According to their genetic mechanisms, organic matter pores can be divided into aligned organic pores within primary organic particles (Figure 6A–E), organic matter cell-cavities pores (Figure 6F,G), organic matter gas pores (Figure 6H) and organic matter shrinkage fractures (Figure 6I). FE-SEM shows that the pore sizes of these organic pores are 90~2000 μm, which is larger than some inorganic pores. The morphology

of organic matter pores is closely related to the structure of primary organic matter, with hydrocarbon generation controlling the early and late appearance of these pores. Aligned organic pores within primary organic particles are generally oval or narrow slit shapes, with the long axes aligned with the direction of organic matter spreading (Figure 6A–E). These aligned pores are largely controlled by the original structure of organic matter. Organic matter cell-cavity pores are developed in organic particles with obvious original structures (Figure 6F,G). Cell-cavity pores in exinite are round and oval, with pore sizes of about 10 μm (Figure 6F), while some slit pores occur along the structure of the organic particles. Organic matter gas pores are mostly round, of various sizes, and are not common in the shale of the Sanzhao area (Figure 6H). These pores are produced after gas is released from organic particles by hydrocarbon generation. Organic matter shrinkage fractures are caused by organic matter shrinkage during hydrocarbon generation in the process of thermal evolution. They are slit pores, occurring along the edges of organic particles (Figure 6I). FE-SEM also shows that all of these organic matter pores are filled with autogenous minerals such as pyrite, chlorite, quartz, and other minerals with good crystal shapes (Figure 6C,D,F,G). These autogenous minerals greatly reduce the numbers of organic matter pores (Figure 6D).
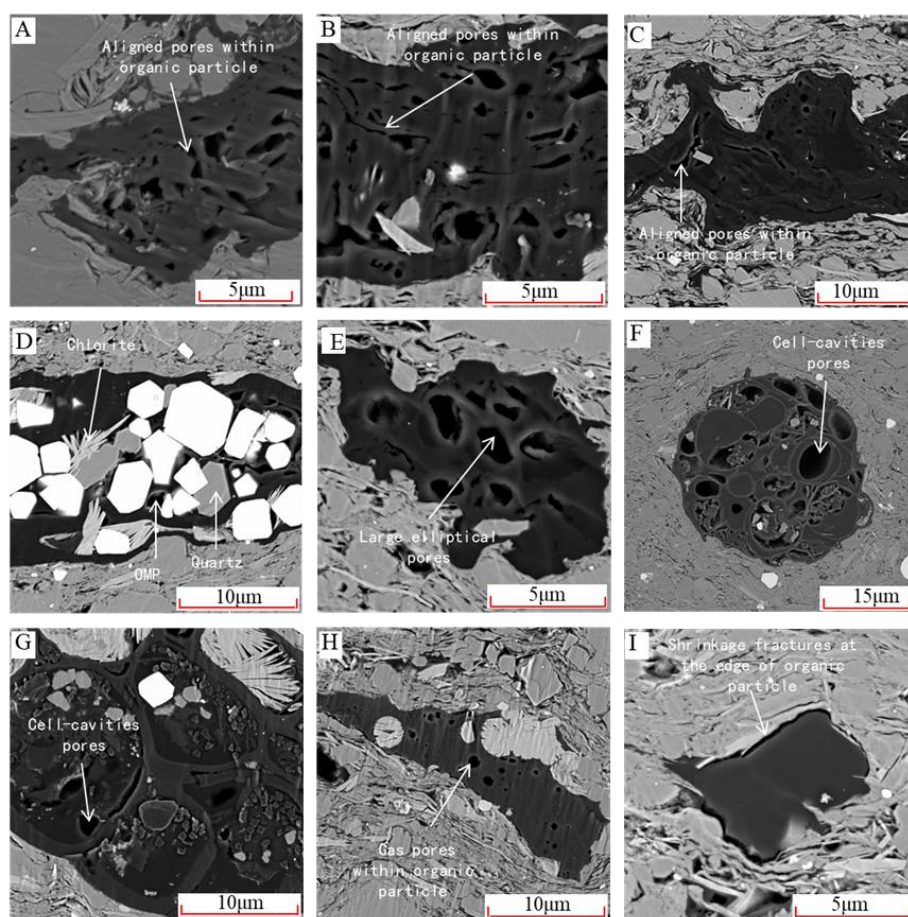

Figure 6. Organic matter pores. (**A–E**) Aligned organic pores. The pores in (**A–C**) are mainly slit pores within organic particles, while the pores of I are large and elliptical. However, all of the pores show alignments that follow the original structure of the organic matter. The organic particles in (**D**) may be the same as those in (**A,B**), which are full of aligned organic pores. However, these pores are filled with pyrite, chlorite, and quartz, which reveal the characteristics of the pores. (**F**) Organic matter cell-cavity pores, which are large and round. The morphology of these pores is controlled by the structure of nearby organic particles and provides a good reflection of their internal structure. (**G**) Cell-cavity pores in exinite. The pores are slit along the edges. (**H**). organic particles with gas pores that vary in size, but are all round in shape. (**I**) Organic particles without internal pores but with shrinkage fractures around their edges.

A large number of FE-SEM scans were carried out, revealing that the shale pores in the Sanzhao area are mainly inorganic mineral pores, mostly relatively well-connected inter-particle pores between grains and clay minerals. Organic matter pores are also developed in organic matter particles, and the pores are mostly micron-sized with fewer rounded gas pores. Organic matter pores inherit the structure and, to some extent, the orientation of the original organic matter.

4.4. Pore Structure Characteristics

4.4.1. Pore Structure Features Based on MAPS Images Analysis

The numbers and pore size distribution of pores in micro-zone facies were calculated using Avizo software to superimpose MAPS images from SEM scans. This method was used to produce large-scale stitched images of six samples from the Sanzhao area. Twenty images were selected for each sample, and a total of 1 million pores were counted. The results show that the pore size distribution (PSD) of shale in Sanzhao area is 10 nm~10,000 nm, consisting mainly of mesopores. Sixty percent of these are between 10~20 nm, followed by 20 nm~30 nm pores, and then 100~200 nm large pores (Figure 7(A-1)). Although pores < 100 nm predominate numerically, the main contributors to pore area are pores with diameters larger than 100 nm. Pores with diameters of 100 nm~300 nm and 1000 nm~2000 nm are the main contributors to surface porosity (Figure 7(A-2,A-3)). Poor image resolution means that the characteristics of pores between 10 and 20 nm cannot be reliably determined, but the rest of the PSD corresponds well with the images.
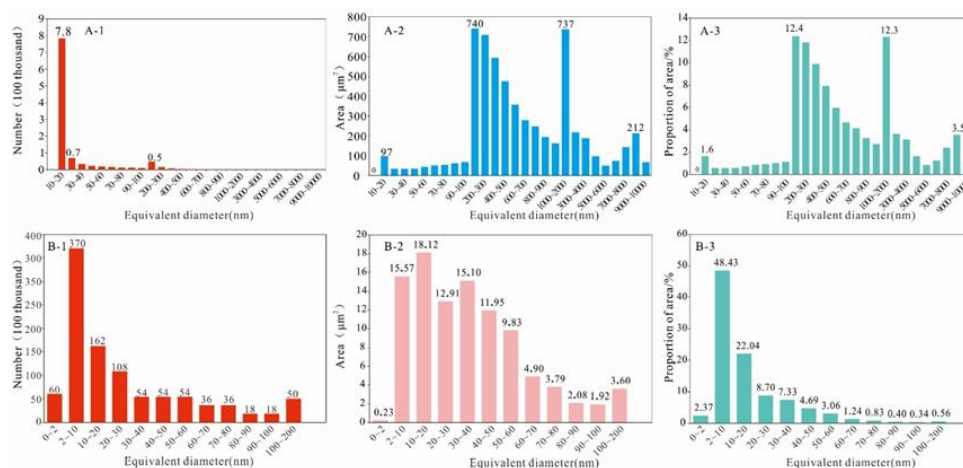

Figure 7. Pore structure characteristics. (**A-1**–**A-3**) is based on MAPS image analysis obtained using AVIZO. The pore size is mainly 10~20 nm, but the pore area is mainly provided by 100~200 nm and 1000~2000 nm pores. (**B-1**–**B-3**) shows the pore size distribution, pore volume, and specific surface area of nitrogen adsorption. The pore size is mainly 2~10 nm, pore area is mainly provided by pores with 2–50 nm.

4.4.2. Pore Structure Characteristics of LPNA

Low-pressure N_2 adsorption-desorption data from 18 samples show that, in the part with high relative pressure (P/P0 > 0.4), the adsorption isotherms of the samples do not coincide with the desorption isotherms. The desorption isotherms are located above the adsorption isotherms, forming a hysteresis loop. According to the classification scheme of IUAPC [43], the N_2 isotherm shapes can indicate 4 types of pores that are H1-both ends open pore(Steep narrowing of hysteresis loop and saturated platform), H2-ink-bottle shaped pore(like H1, but the desorption curve has a longer platform), H3-slit-shaped pore(H3 is found in layered aggregates, the lower limit of the desorption branch is usually located at the P/P0 pressure point caused by the cavitation) and H4-narrow slit-like pore(like H3, but at the lower point of P/P0 there is a very significant adsorption). According to hysteresis loop morphology, the shale pores in Sanzhao are of type H3, mainly slit pores

(Figure 8). DFT pore size analysis shows that the proportions of micropores, mesopores, and macropores in the Qingshankou Formation shale in the Sanzhao area are 2.9%, 74.8%, and 22.3%, respectively. Mesopores of 2~50 nm predominate, with 2~10 nm as the peak of the pore size distribution with the best developed pores. (Figures 7(B-1) and 8). The BET specific surface area results show that the specific pore surface area of the Sanzhao area is 5.4 m^2/g~22.9 m^2/g, with an average of 10.5 m^2/g. Mesopores make up 86.7% of the total specific surface area, with 2~10 nm pores making the largest contribution (44.59%). BJH pore volume shows that the pore volume of the Sanzhao area is 0.03 cm^3/g~0.07 cm^3/g, with an average of 0.05 cm^3/g. Mesopores contribute most to pore volume, accounting for 61.2% of the total pore volume, with 10~20 nm and 30~40 nm pores predominating (Figure 8).
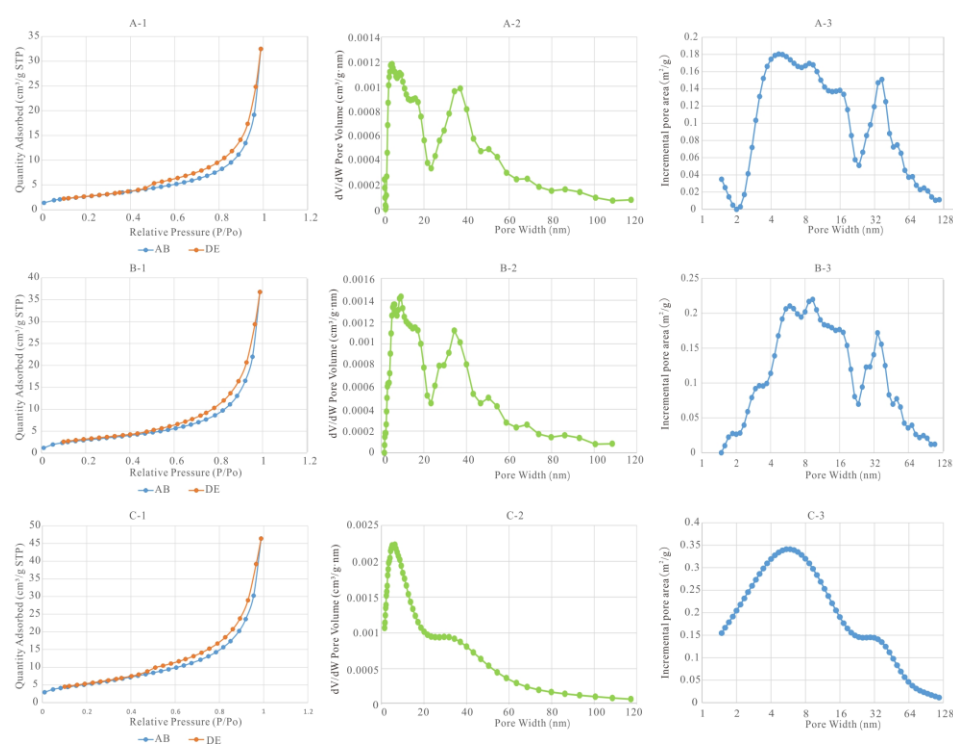

Figure 8. Pore structure characteristics from LPNA. (**A-1**–**A-3**) show the pore structure of massive shale, which pore type is H3. Pore size distribution presents a bimodal pattern, and pores are mainly concentrated at 0~10 nm and 30~40 nm, with 5 nm pores contributing the most to pore volume. The specific surface area showed a bimodal pattern, with 5 and 37 nm pores contributing the most to the area. (**B-1**–**B-3**) show the pore structure of laminated shale, pore volume and surface area are similar to those of massive shale. (**C-1**–**C-3**) show the pore structure of lamellated shale, which shows biggest difference with massive shale and laminated shale. It shows only one peak, 6 nm pores have great contribution to pore volume and surface area.

5. Discussion

5.1. Pore Characteristic of Shale with Different Sedimentary Sturctures

The shales in the Sanzhao area can be divided into massive shale, laminated shale, and lamellated shale according to sedimentary structure (3.2). Massive shale has the smallest pore volume (0.049 cm^3/g), laminated shale has a slightly larger pore volume (0.0543 cm^3/g), and lamellated shale has the largest pore volume (0.07 cm^3/g) (Figure 8). The distribution of pore volumes is similar to the pore size distribution. The volumes of 2~16 nm and 23~37 nm pores increase with an increase in pore size. The volumes of 16~23 nm and 37~128 nm pores tend to decrease, with 37 nm pores making the largest contribution. The specific surface areas of massive shale, laminated shale, and lamellated shale are 5.632 m^2/g, 6.3 m^2/g and 11.024 m^2/g, respectively, Again, massive shale is the

smallest and lamellated shale is the largest (Figure 8). The pore structure characteristics of the shales display different curve characteristics in different sedimentary formations. Massive shale has the largest proportion of pores at 4.4 nm (0.18 m^2/g). Pores of 8.6 nm in laminated shale contribute the largest increment of specific surface area (0.22 m^2/g). Pores of 5.03 nm contribute most to the surface (0.35 m^2/g). The total pore volume and specific surface area of the shale are large, and the pores are well developed.

5.2. Controls of Pore Structure

5.2.1. Influence of Mineral Composition and Laminar Structure

Under FE-SEM, pore development in felsic laminae is seen to be significantly different from that of clay laminae. Mineral particles in felsic laminae are filled with authigenic chlorite, so that the pores in the laminae are smaller and less developed. In clay laminae, interparticle pores occur widely between clay minerals and between grains and clay minerals. Pore connectivity is good, and the reservoir properties appear to be better (Figure 9(A-1,A-2,B-1,B-2)). Shale samples with both felsic and clay laminae were selected, and, based on MAPS images, the pore size distributions and surface areas of the two lamina types were calculated. The results show that pore size distribution in felsic and clay laminae is basically the same. Pores of 10~20 nm, 20~30 nm, and 100~200 nm predominate, with pores of 100~400 nm contributing nearly 50% of the surface area (Figure 9(A-3,A-4,B-3,B-4)). However, the number of pores developed in clays within the same horizon is three times that of felsic laminae, with better pore connectivity and reservoir properties. In Figure 10, A and C correspond to the felsic laminae and clay laminae in Figure 9, respectively, and show an extraordinary difference in specific surface areas. The specific surface areas of clay laminae are substantially larger than those of felsic laminae.
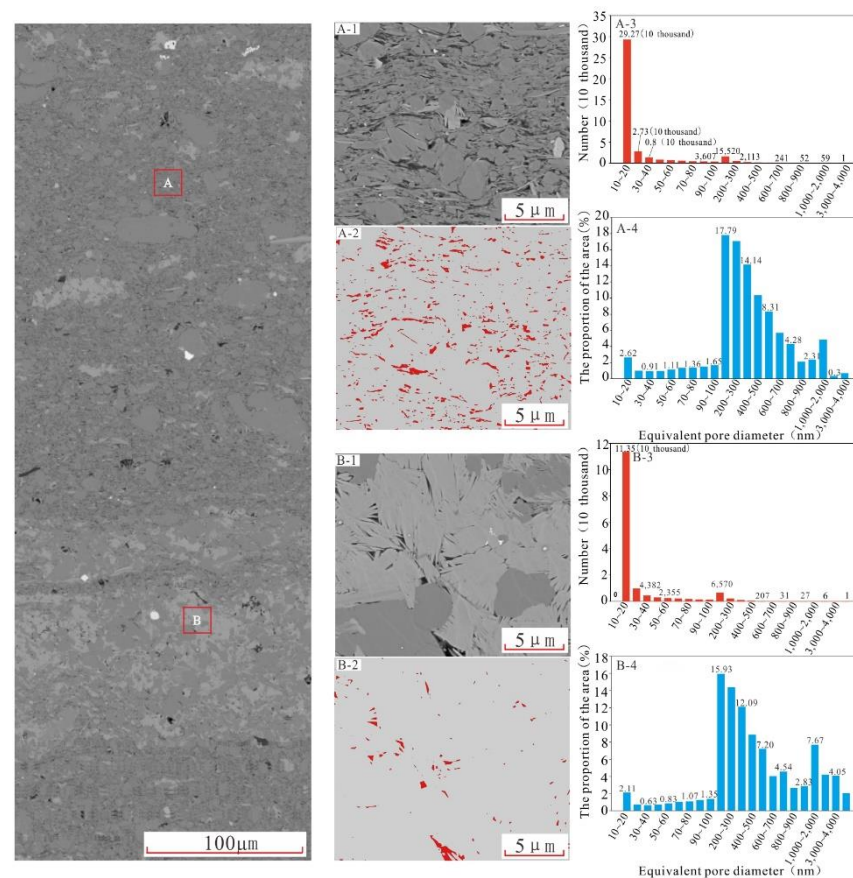

Figure 9. Comparison of pore structure characteristics between felsic and clay laminae. (**A**) represents the region of clay laminae within which pores are greatly developed; (**B**) represents the represents the region of felsic laminae. Pores between grains are filled with authigenic chlorite, which makes the laminae dense.
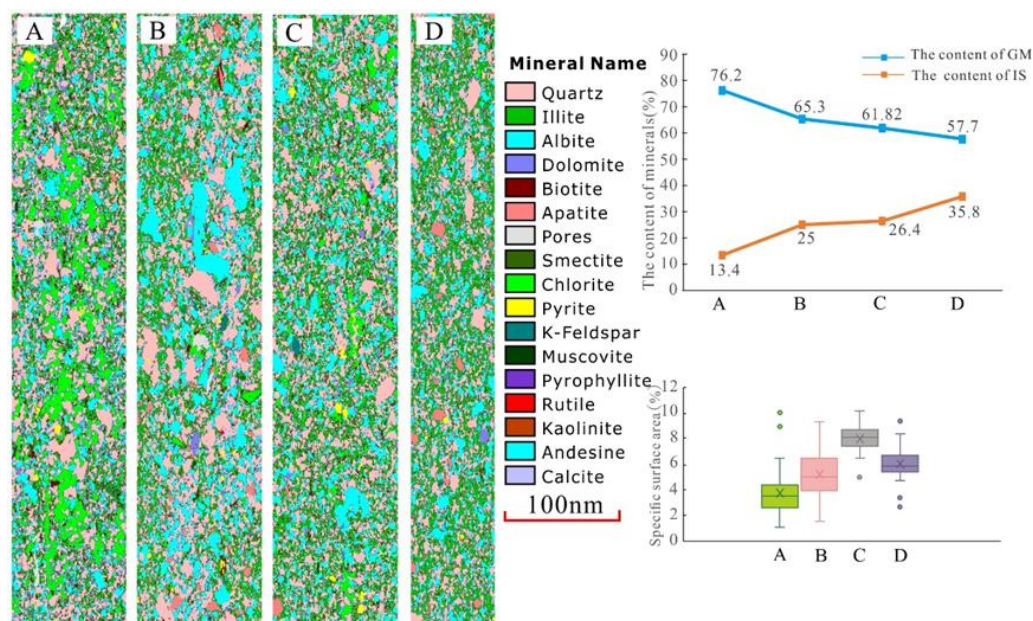
Figure 10. Influence of granular minerals and IS clay content on specific surface area. (**A**,**C**)are No. 7 samples, TOC is 6.54%, (**A**) is felsic laminar, (**C**) is clay laminar. (**B**,**D**) are samples No. 10, TOC is 6.58%, (**B**) is felsic lamination, (**D**) is clay lamination.

It has been found in previous studies that higher contents of illite and illite/smectite mixed layer (IS) at depths greater than 3500 m are conducive to pore development [44], which accords with the results of this study. However, it was observed that the clay layers in some samples with high IS contents were dense and the pores were less developed. However, in other samples, clay laminae containing grains have numerous pores. It seems that there is an ideal balance in the relative proportions of IS and grain minerals in mud shales that is most conducive to pore development. IS is particularly developed in clay laminae, and grain minerals are particularly developed in felsic laminae. In order to confirm whether this phenomenon also occurs in the Sanzhao area, the specific surface areas of two shale samples with similar TOC contents and with both felsic and clays laminae were calculated. The IS and grain particle contents of each lamina were also calculated (Figure 10). It was found that the specific surface area of felsic laminae in both samples is lower than that of clay minerals and correlates closely with the contents of IS and grain particles. The specific surface area was obtained using Avizo's processing of MAPS images, and the content of IS and grain minerals were obtained by QEMSCAN. The results show that, with a decrease in particle content, the content of IS increases, as does the specific surface area. The specific surface area is highest when grain mineral content reaches 60% and IS content is 25%. As grain mineral content continues to decrease and IS content continues to increase, the specific surface area decreases. It can therefore be inferred that a mineral composition with 60% grain mineral content and 25% IS content is the best combination for pore development. However, it must be pointed out that this applies when pores are relatively dense and when intergranular felsic laminae are filled with cementation or clay mineral chlorite, which are considered to be included in the particle content.

5.2.2. Influence of TOC Content

TOC content makes an important contribution to the porosity of shale reservoirs and is the main controlling factor affecting the volume, specific surface area, and porosity of shale nanopores. In general, TOC content is positively correlated with the pore volume and specific surface area of mesopores [23,24]. However, the pore volumes and specific surface areas of shales in the Sanzhao area are negatively correlated with TOC content, while pore size is positively correlated with TOC content (Figure 11). This indicates that pores related to organic matter in this area are generally large (Figures 6 and 7). TOC content has a

particularly significant impact on organic pores. Milliken et al. used FE-SEM to study the Marcellus shale reservoir in Pennsylvania, USA, and found that when TOC < 5.5% it was positively correlated with organic pores, but that when TOC exceeded 5.5%, there was no obvious correlation with organic pores [45,46]. For shales that have reached the oil generation window, the higher the TOC content the better the pore structure parameters. Of course, at the peak of oil generation (Ro = 0.85~1.1%), the formation of organic pores gradually decreases as residual bitumen fills some of the pore space [11,28,29]. This also explains the negative correlation of TOC content with pore volume and specific surface area in the Sanzhao area. Avizo software was used to process MAPS images of five samples in the Sanzhao area. The results show the specific surface areas of samples with different maturity levels in the Sanzhao area, with Ro between 0.9% and 1.0% (shown in the shaded part of Figure 12a). This demonstrates that specific surface area decreases with decreasing TOC content. However, the pore area identified by MAPS image processing included a large proportion of pores larger than 100 nm (Figure 7(A-1–A-3)). Of these, the sample with a TOC of 6.54% has a higher specific surface area than the sample with a TOC of 6.58% because of the different effects of the mineral components at the same TOC.
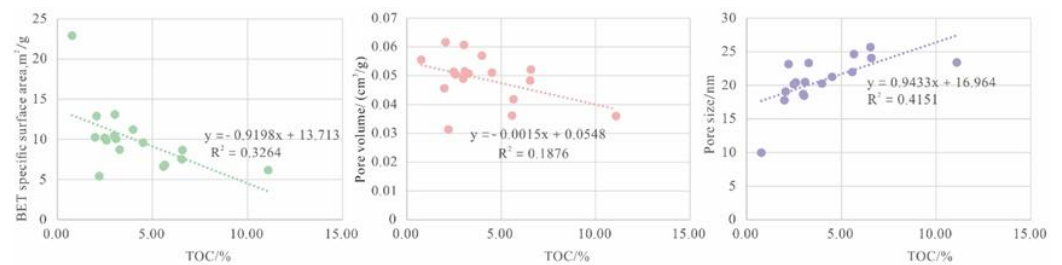

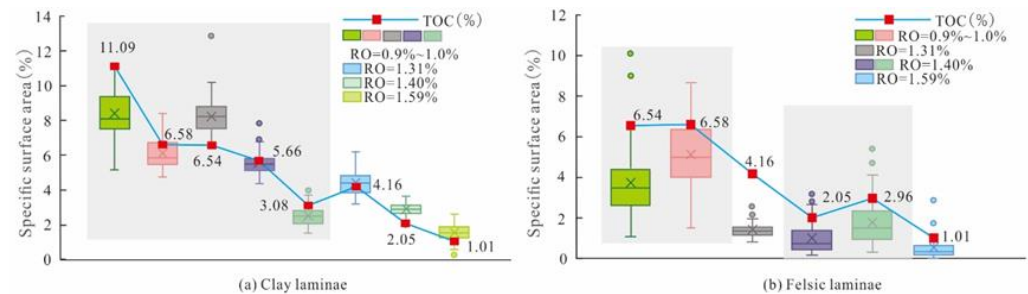**Figure 11.** Relationship between TOC and pore structure.

Figure 12. Relationship between maturity and specific surface area.in clay laminae. (**a**) The first five samples were low-mature and from the Sanzhao area, followed by 3 high-mature samples from the Gulong area with Ro = 1.31%, 1.40% and 1.59%. Samples with 1.31%and 1.40% Ro have higher SSA than that of sample with 0.9~1.0% Ro, 3.08% TOC. (**b**) in felsic laminae, two groups of samples with the same Ro (0.9~1.0% Ro and 1.40% Ro), and high TOC contents have high SSA. Two samples with 1.40% Ro have higher SSA than that of the sample with 1.31% Ro, even though the latter has high TOC content.

5.2.3. Influence of Maturity

Changes in the reservoir space structure of shale are the result of the decomposition of organic matter during thermal maturation. With increasing maturity, organic matter pores increase gradually, and the pore sizes become larger, reaching a peak at the peak of oil generation (Ro = 0.8–1.2%). After this, organic matter pores decrease slightly. However, organic matter pores appear again in large numbers with the cracking of crude oil [28,29,47]. At the over-mature stage (Ro > 2%), the generation of OM pores reaches its upper limit, and the volume and surface area of OM pores thereafter decrease with increasing thermal maturity [32,48]. As organic matter decomposes, it also has an effect on diagenetic fluids and inorganic pores. In order to demonstrate the influence of thermal maturity on the pore structure of the Qingshankou Formation shale, three shale samples with high maturity

(RO 1.31%, 1.40%, and 1.59%) from the Gulong area and five samples with relatively low maturity (RO 0.9–1.0%) from the Sanzhao area were selected for comparison. Due to the difference in pore structure between the clay and felsic laminae, the differences in specific surface area between the two types of lamina at different stages of maturity were calculated separately. The results show that high-mature shales with similar TOC contents (Ro = 1.3%, 1.4%) have a higher specific surface area in both clay and felsic laminae, and the high-mature shales (Ro = 0.9–1.0%) in clay laminae have a higher specific surface area in the samples with a TOC of 3.08%. The specific surface area of the shale with Ro = 1.4% (TOC = 2.96%) is higher than that of the shale with Ro = 1.31% (TOC = 4.16%) in the felsic laminae. The difference in specific surface area between the two groups of samples with the same maturity (Ro of 0.9% to 1.0% and Ro of 1.4%) in the felsic laminae is due to the higher grain mineral content and TOC content in the former group. The specific surface area of samples (Ro = 1.0–1.4%) increased with the increase in thermal evolution, mainly because: (1) secondary pores were formed by clay mineral transformation; and (2) pores covered by solid bitumen in the early stage were released due to hydrocarbon generation from organic matter, creating a large number of organic matter pores [28,29,31,47].

5.2.4. Influence of Diagenesis

(1)   The transformation of clay minerals

The transformation of clay minerals is an important diagenesis in shale reservoirs with high clay mineral content (up to 79%) in the Qingshankou Formation. In the process of diagenesis, kaolinite and smectite were gradually transformed into illite and chlorite, with an illite/smectite mixed layer and a chlorite/smectite mixed layer as intermediate products [29]. The transformation of clay minerals in the Sanzhao area involved smectite illitization and chloritization, so the compositions of clay minerals include an illite/smectite mixed layer, illite, and chlorite. High contents of the illite/smectite mixed layer and illite are conducive to pore development, particularly in shallow buried shales (<3500 m) with high clay contents and higher porosity. This has been verified in previous studies [32]. Pores between clay platelets in the illite/smectite mixed layer in the Sanzhao area provide good pore spaces for organic matter and good connectivity (Figure 4I). However, chlorite appears as pore linings and also fills pores and blocks pore throats, reducing pore space (Figures 4C–E and 6G). It is also a significant cause of smaller pores in felsic laminae (Figure 9A).

(2)   Dissolution

Dissolution is common in shale samples in the Sanzhao area. Dissolution pores are mainly generated in the interiors and at the edges of unstable minerals by the action of acidic media or organic acids [49,50]. K-feldspar is the main dissolved mineral in the Sanzhao area, as dissolution rarely occurs in carbonate minerals. The K-feldspar has undergone strong dissolution. Large areas of dissolution occur at the edges and in the interiors of mineral particles, forming irregular pores with micron-scale diameters. Most of the pores are interconnected. FE-SEM shows that these dissolved pores are all filled with large amounts of black organic matter (Figure 5E–G). Dissolution of K-feldspar is related to hydrocarbon generation from organic matter. This produces large amounts of organic acids, which dissolve the K-feldspar [51]. The organic matter that fills the pores further dissolves the K-feldspar as it decomposes. Dissolution of carbonate minerals is less, with only a few dolomites and ankerite having small, isolated pores. Ankerite shows bright edges and dark centers under SEM, with the dissolution of the dark centers being stronger than the bright edges. Dissolution plays an active role in pore development, but the content of K-feldspar and other minerals prone to dissolution is small in the Sanzhao area, so the contribution of dissolution to improving reservoir physical properties is limited.

(3)   Cementation

Shale cementation in the Sanzhao area includes clay mineral cementation, siliceous cementation, carbonate cementation, and pyrite cementation. Clay mineral cementation mainly takes the form of autogenic chlorite filling in felsic intergranular pores, or in the form

of pore linings, completely filling tight reservoirs or partially filling residual intergranular pores (Figures 4C–H and 6D). Autogenetic pyrite develops around the edges of grain minerals in the form of single crystals or framboidal pyrites (Figures 4F, 5B,D and 6D). Small amounts of calcite cementation are observed among mineral grains within felsic laminae, which develop as grains or mosaics at the edges of the felsic grains while dolomite develops as rhombic autocrysts between the grains. (Figure 4A,F). Siliceous cements in shale mainly exist in the form of automorphic quartz crystals between clay minerals or in the form of quartz microcrystals between pores [50] (Figures 4C–E,H and 6D). The sizes of quartz crystals vary greatly, from up to 60 μm and down to less than 1 μm. Authigenic quartz crystals derive from the dissolution and reprecipitation of the original quartz particles or from smectite illitization [52–54]. In the Sanzhao area, quartz crystals are mostly developed in the clay layer or in association with chlorite. The two are interlaid, so it is presumed that early mineral dissolution formed chlorite and quartz at the same time (Figure 4D). Cementation of shale has a dual effect, reducing porosity and impairing reservoir physical properties while increasing the compaction resistance and brittleness of the reservoir [55].

(4)   Hydrocarbon generation from organic matter

In the process of hydrocarbon generation, organic matter is transformed from amorphous organic matter with sulfur and oxygen-rich aliphatic kerogen (Alginite liptodetrinite) in its low maturity state into solid bitumen and liquid hydrocarbon when mature. It becomes increasingly aromatized after thermal maturation and finally evolves into pyrobitumen [56,57]. During this process, the maceral components of organic matter change from yellow-green fluorescence under a fluorescence microscope when low-mature to having no obvious fluorescence when high-mature [28]. Hydrocarbon generation changes the composition of shale, producing large numbers of organic pores, which become an important pore type in shale. Some scholars believe that maturity has little influence on inorganic mineral pores [32]. However, the interaction between hydrocarbon generation from organic matter and inorganic minerals has increasingly attracted attention [51,55,58]. There is no doubt that organic matter and inorganic minerals interact during diagenesis. Organic acids produced by hydrocarbon generation from organic matter dissolve unstable minerals (feldspar, carbonate minerals, clay minerals) and form dissolution pores. The ions produced (K, Mg, Ca, and Fe) promote the transformation of clay minerals. This process leads to the precipitation of large amounts of Si, resulting in the formation of autogenous quartz and the transformation of clay minerals. The organic matter in the Qingshankou Formation shale in the Sanzhao area is middle- to high-mature. As thermal evolution proceeds, algae, amorphous matter, and clastic shells gradually transform into solid bitumen and oil, with the formation of large numbers of organic pores within organic matter particles (Figure 6). As it interacts with inorganic minerals, the organic matter in the dissolution pores itself generates a large number of organic matter pores and thus promotes further pore dissolution (Figure 5E–G).

6. Conclusions

1. The Qingshankou Formation shale in the Sanzhao area is composed of relatively pure clay shale with high TOC content and high hydrocarbon generation potential. The shale is predominantly composed of clay minerals, quartz, and feldspar, with small amounts of ferric dolomite, calcite, and pyrite. The clay minerals are mainly an illite/smectite mixed layer, followed by illite and small amounts of chlorite.
2. FE-SEM shows that there are interparticle pores, intraparticle pores, and organic pores in the Qingshankou Formation shale. Of the three types, interparticle pores are the smallest but the most developed, particularly those related to clay minerals. Pyrite interparticle pores and intraparticle dissolved pores have large pore sizes and are mostly filled with organic matter. Occasional fossil-cavity pores are found, which are full of organic matter and oil film. Organic matter is abundant in the shale, which provides good conditions for the development of organic matter pores. A few of the organic matter pores are gas pores, and most are produced as oval or aligned pores.

They often have a marked alignment, which is related to the original structure and compaction of organic matter.

3. LPNA pore structure analysis shows that shale pores in the Sanzhao area are of type H3 and are mostly slit pores. The specific surface areas are 5.4~22.9 m^2/g, with an average of 10.5 m^2/g. Pore volumes are 0.03 m^2/g~0.07 cm^3/g, with an average of 0.05 cm^3/g. Mesopores contribute most to the pore volume and surface area. MAPS images show that the pore size distribution of shale is mainly 20 nm~30 nm and 100 nm~200 nm, and that large pores, particularly 100~200 nm and 1~2 μm, make the largest contribution to the specific surface area. The total pore volume and the specific surface area of lamellated shale are larger than those of massive and laminated shale, and pore development is better.

4. The factors controlling shale pore structure are discussed in four aspects: mineral composition, organic matter content, maturity, and diagenesis. The relative contents of clay IS and granular minerals (felsic, dolomite, calcite, pyrite, etc.) have an important influence on pore development. Pore development is best when the content of granular minerals is 60% and that of IS is 25%. TOC content is negatively correlated with the specific surface areas and pore volumes of micro- and mesopores and positively correlated with the specific surface area of macropores. The transformation of clay minerals and hydrocarbon generation from organic matter caused an increase in the specific surface area. Clay mineral transformation and dissolution and hydrocarbon generation from organic matter are conducive to pore development, and cementation makes felsic laminae denser.

Author Contributions: Conceptualization, Methodology, Writing—Original draft preparation, S.Z.; funding acquisition, S.W.; supervision, R.Z.; validation, J.Z. and C.L.; resources, T.Z.; investigation, Y.C., M.L., G.H., Y.K. and B.W. All authors have read and agreed to the published version of the manuscript.

Data Availability Statement: The data presented in this study are available on request from the corresponding author.

Conflicts of Interest: The authors declare no conflict of interest.

References

1. Passey, Q.R.; Bohacs, K.M.; Esch, W.L.; Klimentidis, R.; Sinha, S. From Oil-Prone Source Rock to Gas-Producing Shale Reservoir—Geologic and Petrophysical Characterization of Unconventional Shale-Gas Reservoirs. In Proceedings of the International Oil and Gas Conference and Exhibition in China, Beijing, China, 8–10 June 2010; OnePetro: Richardson, TX, USA, 2010.
2. Singh, P.; Roger, S.; Borges, G.; Perez, R.; Portas, R.; Marfurt, K. Reservoir Characterization of Unconventional Gas Shale Reservoirs: Example from the Barnett Shale, Texas, USA. *Okla. City Geol. Soc.* **2008**, *60*, 15–31.
3. Zou, C.N.; Dong, D.Z.; Wang, Y.M.; Liu, X.J.; Huang, J.; Wang, S.F.; Guan, Q.Z.; Zhang, C.C.; Wang, H.Y.; Liu, H.L.; et al. Shale gas in China: Characteristics, challenges and prospects (I). *Pet. Explor. Dev.* **2015**, *42*, 689–701. [CrossRef]
4. Zou, C.; Dong, D.; Wang, Y.; Li, X.; Huang, J.; Wang, S.; Guan, Q.; Zhang, C.; Wang, H.; Liu, H.; et al. Shale gas in China: Characteristics, challenges and prospects (II). *Pet. Explor. Dev.* **2016**, *43*, 182–196. [CrossRef]
5. Bustin, R.M.; Bustin, A.M.M.; Cui, X.; Ross, D.J.K.; Pathi, V.S.M. Impact of Shale Properties on Pore Structure and Storage Characteristics. In Proceedings of the All Days, Fort Worth, TX, USA, 16 November 2008; SPE: Fort Worth, TX, USA, 2008. Paper No. SPE-119892-MS.
6. Loucks, R.G.; Reed, R.M.; Ruppel, S.C.; Hammes, U. Spectrum of Pore Types and Networks in Mudrocks and a Descriptive Classification for Matrix-Related Mudrock Pores. *Bulletin* **2012**, *96*, 1071–1098. [CrossRef]
7. Loucks, R.G.; Reed, R.M.; Ruppel, S.C.; Jarvie, D.M. Morphology, Genesis, and Distribution of Nanometer-Scale Pores in Siliceous Mudstones of the Mississippian Barnett Shale. *J. Sediment. Res.* **2009**, *79*, 848–861. [CrossRef]
8. Ross, D.J.K.; Bustin, M.R. The Importance of Shale Composition and Pore Structure upon Gas Storage Potential of Shale Gas Reservoirs. *Mar. Pet. Geol.* **2009**, *26*, 916–927. [CrossRef]
9. Zou, C.; Zhu, R.K.; Bai, B.; Yang, Z.; Wu, S.T.; Su, L.; Dong, D.Z.; Li, X.J. First discovery of nano-pore throat in oil andgas reservoir in China and its scientific value. *Acta Petrol. Sin.* **2011**, *27*, 1857–1864.

10. Tian, H.; Zhang, S.; Liu, S.; Zhang, H. Determination of organic-rich shale pore features by mercury injection and gas adsorption methods. *Acta Pet. Sin.* **2012**, *33*, 419–427.

11. Mastalerz, M.; Schimmelmann, A.; Drobniak, A.; Chen, Y.Y. Porosity of Devonian and Mississippian New Albany Shale across a Maturation Gradient: Insights from Organic Petrology, Gas Adsorption, and Mercury Intrusion. *Bulletin* **2013**, *97*, 1621–1643. [CrossRef]

12. Tian, H.; Pan, L.; Xiao, X.M.; Wilkins, R.W.T.; Meng, Z.P.; Huang, B.J. A Preliminary Study on the Pore Characterization of Lower Silurian Black Shales in the Chuandong Thrust Fold Belt, Southwestern China Using Low Pressure N_2 Adsorption and FE-SEM Methods. *Mar. Pet. Geol.* **2013**, *48*, 8–19. [CrossRef]

13. Wang, X.J.; Wang, M.; Li, Y.; Zhang, J.X.; Li, M.; Li, Z.; Guo, Z.Q.; Li, J.B. Shale Pore Connectivity and Influencing Factors Based on Spontaneous Imbibition Combined with a Nuclear Magnetic Resonance Experiment. *Mar. Pet. Geol.* **2021**, *132*, 105239. [CrossRef]

14. Yang, F.; Ning, Z.F.; Kong, D.T.; Liu, H.Q. Characterization of microscopic pore structures in shale reservoirs. *Nat. Gas Geosci.* **2013**, *24*, 450–455.

15. Zheng, X.W.; Zhang, B.Q.; Sanei, H.; Bao, H.Y.; Meng, Z.Y.; Wang, C.; Li, K. Pore Structure Characteristics and Its Effect on Shale Gas Adsorption and Desorption Behavior. *Mar. Pet. Geol.* **2019**, *100*, 165–178. [CrossRef]

16. Yang, C.; Xiong, Y.Q.; Zhang, J.C. A Comprehensive Re-Understanding of the OM-Hosted Nanopores in the Marine Wufeng–Longmaxi Shale Formation in South China by Organic Petrology, Gas Adsorption, and X-ray Diffraction Studies. *Int. J. Coal Geol.* **2020**, *218*, 103362. [CrossRef]

17. Milner, M.; McLin, R.; Petriello, J. Imaging Texture and Porosity in Mudstones and Shales: Comparison of Secondary and Ion-Milled Backscatter SEM Methods. In Proceedings of the All Days, Calgary, AB, Canada, 19 October 2010; SPE: Calgary, AB, Canada, 2010. Paper No. SPE-138975-MS.

18. Wang, P.F.; Jiang, Z.X.; Ji, W.M.; Zhang, C.; Yuan, Y.; Chen, L.; Yin, L.S. Heterogeneity of Intergranular, Intraparticle and Organic Pores in Longmaxi Shale in Sichuan Basin, South China: Evidence from SEM Digital Images and Fractal and Multifractal Geometries. *Mar. Pet. Geol.* **2016**, *72*, 122–138. [CrossRef]

19. Wei, S.L.; He, S.; Pan, Z.J.; Zhai, G.Y.; Dong, T.; Guo, X.W.; Yang, R.; Han, Y.J.; Yang, W. Characteristics and Evolution of Pyrobitumen-Hosted Pores of the Overmature Lower Cambrian Shuijingtuo Shale in the South of Huangling Anticline, Yichang Area, China: Evidence from FE-SEM Petrography. *Mar. Pet. Geol.* **2020**, *116*, 104303. [CrossRef]

20. Tian, S.S.; Bowen, L.; Liu, B.; Zeng, F.; Xue, H.T.; Erastova, V.; Greenwell, H.C.; Dong, Z.T.; Zhao, R.X.; Liu, J.Z. A Method for Automatic Shale Porosity Quantification Using an Edge-Threshold Automatic Processing (ETAP) Technique. *Fuel* **2021**, *304*, 121319. [CrossRef]

21. Guo, X.S.; Li, Y.P.; Liu, R.B.; Wang, Q.B. Characteristics and controlling factors of micro-pore structures of Longmaxi Shale Play in the Jiaoshiba area, Sichuan Basin. *Nat. Gas Ind.* **2014**, *34*, 9–16.

22. Ji, L.M.; Qiu, J.L.; Xia, Y.Q.; Zhang, T.W. Micro-pore characteristics and methane adsorption properties of common clay minerals by electron microscope scanning. *Acta Pet. Sin.* **2012**, *33*, 249–256.

23. Chen, L.; Jiang, Z.X.; Liu, K.Y.; Tan, J.Q.; Gao, F.L.; Wang, P.F. Pore Structure Characterization for Organic-Rich Lower Silurian Shale in the Upper Yangtze Platform, South China: A Possible Mechanism for Pore Development. *J. Nat. Gas Sci. Eng.* **2017**, *46*, 1–15. [CrossRef]

24. Xu, L.W.; Liu, L.F.; Jiang, Z.X.; Chen, L.; Wang, Y. Methane Adsorption in the Low–Middle-Matured Neoproterozoic Xiamaling Marine Shale in Zhangjiakou, Hebei. *Aust. J. Earth Sci.* **2018**, *65*, 691–710. [CrossRef]

25. Cao, T.T.; Song, Z.G.; Wang, S.B.; Cao, X.X.; Li, Y.; Xia, J. Characterizing the Pore Structure in the Silurian and Permian Shales of the Sichuan Basin, China. *Mar. Pet. Geol.* **2015**, *61*, 140–150. [CrossRef]

26. Wei, X.F.; Liu, R.B.; Zhang, T.S.; Liang, X. Micro-scale pore structure characteristics and development control factors of shale gas reservoir: A case of Longmaxi Formation in XX area southern Sichuan and norhtern Guizhou. *Nat. Gas Geosci.* **2013**, *24*, 1048–1059.

27. Curtis, M.E.; Cardott, B.J.; Sondergeld, C.H.; Rai, C.S. Development of Organic Porosity in the Woodford Shale with Increasing Thermal Maturity. *Int. J. Coal Geol.* **2012**, *103*, 26–31. [CrossRef]

28. Liu, B.; Wang, Y.; Tian, S.S.; Guo, Y.L.; Wang, L.; Yasin, Q.; Yang, J.G. Impact of Thermal Maturity on the Diagenesis and Porosity of Lacustrine Oil-Prone Shales: Insights from Natural Shale Samples with Thermal Maturation in the Oil Generation Window. *Int. J. Coal Geol.* **2022**, *261*, 104079. [CrossRef]

29. Teng, J.; Deng, H.C.; Liu, B.; Chen, W.L.; Fu, M.Y.; Xia, Y.; Yu, H.Z. Insights of the Pore System of Lacustrine Shales from Immature to Late Mature with the Aid of Petrology, Mineralogy and Porosimetry: A Case Study of the Triassic Yanchang Formation of the Ordos Basin, North China. *J. Pet. Sci. Eng.* **2021**, *196*, 107631. [CrossRef]

30. Dong, T.; Harris, N.B. The Effect of Thermal Maturity on Porosity Development in the Upper Devonian–Lower Mississippian Woodford Shale, Permian Basin, US: Insights into the Role of Silica Nanospheres and Microcrystalline Quartz on Porosity Preservation. *Int. J. Coal Geol.* **2020**, *217*, 103346. [CrossRef]

31. Löhr, S.C.; Baruch, E.T.; Hall, P.A.; Kennedy, M.J. Is Organic Pore Development in Gas Shales Influenced by the Primary Porosity and Structure of Thermally Immature Organic Matter? *Org. Geochem.* **2015**, *87*, 119–132. [CrossRef]

32. Zhang, Y.F.; Yu, B.S.; Pan, Z.J.; Hou, C.H.; Zuo, Q.W.; Sun, M.D. Effect of Thermal Maturity on Shale Pore Structure: A Combined Study Using Extracted Organic Matter and Bulk Shale from Sichuan Basin, China. *J. Nat. Gas Sci. Eng.* **2020**, *74*, 103089. [CrossRef]

33. Feng, Z.Q.; Jia, C.Z.; Xie, X.N.; Zhang, S.; Feng, Z.H.; Cross, T.A. Tectonostratigraphic Units and Stratigraphic Sequences of the Nonmarine Songliao Basin, Northeast China. *Basin Res.* **2010**, *22*, 79–95. [CrossRef]

34. Li, J.; Shu, L.S. Mesozoic-Cenozoic Tectonic Features and Evolution of the Song-Liao Basin, NE China. *J. Nanjing Univ.* **2002**, *38*, 525–531.

35. Li, Z.A. Evolutionary characteristics of mantle heat flow in the Songliao Basin. *Geotecton. Metallog.* **1995**, *19*, 104–112. [CrossRef]

36. Li, X.W. Numerical simulations of the burial & thermal histories for Daqing Placanticline in north Songliao Basin. *Pet. Geol. Oilfield Dev. Daqing* **2015**, *34*, 46–50.

37. Ren, Z.L.; Xiao, D.M.; Chi, Y.L. Restoration of the palaeogeotherm in Songliao Basin. *Pet. Geol. Oilfield Dev. Daqing* **2001**, *20*, 13–14.

38. Fu, G.; Wang, Y.G. Downward "backfilling" transport of oil from source rocks of the Qingshankou Formation in the Sanzhao Depression and its significance. *Acta Sedimentol. Sin.* **2008**, *26*, 355–360.

39. Chi, Y.L.; Xiao, D.M.; Yin, J.G. The "injection" reservoir formation mechanism in the Sanzhao area of the Songliao Basin. *Acta Geol. Sin.* **2000**, *74*, 371–377.

40. Liu, C.; Xu, X.Y.; Liu, K.Y.; Bai, J.; Liu, W.B.; Chen, S. Pore-Scale Oil Distribution in Shales of the Qingshankou Formation in the Changling Sag, Songliao Basin, NE China. *Mar. Pet. Geol.* **2020**, *120*, 104553. [CrossRef]

41. Zhou, Y.; Littke, R. Numerical Simulation of the Thermal Maturation, Oil Generation and Migration in the Songliao Basin, Northeastern China. *Mar. Pet. Geol.* **1999**, *16*, 771–792. [CrossRef]

42. Jiao, F.Z.; Zou, C.N.; Yang, Z. Geological theory and exploration & development practice of hydrocarbon accumulation inside continental source kitchens. *Pet. Explor. Dev.* **2020**, *47*, 1147–1159. [CrossRef]

43. Sing, K.S.; Everett, D.H.; Haul, R.A.W.; Moscou, L.; Pierotti, R.A.; Rouquerol, J.; Siemieniewsha, T. Reporting physisorption data for gas/solid systems with special reference to the determination of surface area and porosity. *Pure Appl. Chem.* **1985**, *57*, 603–619. [CrossRef]

44. Zhuo, X.Z.; Hu, Q.H.; Zhang, J.J.; Zhang, L.Y.; Chen, X.S.; Ma, L.C. Conceptual Models for Correlation between Detrital Particles Contents and Pore Distribution of Shale: Taking the Silurian Longmaxi Formation in northwestern Guizhou as an example. *Acta Sedimentol. Sin.* **2018**, *36*, 969–980. [CrossRef]

45. Milliken, K.; Rudnicki, M.; Awwiller, D.N.; Zhang, T.W. Organic Matter–Hosted Pore System, Marcellus Formation (Devonian), Pennsylvania. *AAPG Bull.* **2013**, *97*, 177–200. [CrossRef]

46. Zhang, P.P.; Liu, X.P.; Wang, Y.J.; Sun, X.J. Research progress in shale nanopores. *Adv. Earth Sci.* **2014**, *29*, 1242–1249.

47. Gao, Z.Y.; Xuan, Q.X.; Hu, Q.H.; Jiang, Z.X.; Liu, X.X. Pore Structure Evolution Characteristics of Continental Shale in China as Indicated from Thermal Simulation Experiments. *Bulletin* **2021**, *105*, 2159–2180. [CrossRef]

48. Yang, X.G.; Guo, S.B. Porosity Model and Pore Evolution of Transitional Shales: An Example from the Southern North China Basin. *Pet. Sci.* **2020**, *17*, 1512–1526. [CrossRef]

49. Zhang, S.; Liu, H.M.; Wang, Y.S.; Zhang, B.Q.; Zhang, K.; Wang, M.; Wang, Y.; Fu, A.B.; Bao, Y.S. Diagenetic event of Paleogene shale and its influence on development characteristics of shale pore space in Dongying Sag. *Pet. Geol. Recovery Effic.* **2019**, *26*, 109–118. [CrossRef]

50. Zhao, D.F.; Guo, Y.H.; Bao, Y.J.; Wang, S.Y.; Mao, X.X.; Li, M. Shale reservoir diagenesis and its impacts on pores of the Lower Silurian Longmaxi Formation in southeastern Chongqing. *J. Palaeogeogr.* **2016**, *18*, 843–856.

51. Wu, L.G.; Guo, X.S.; Guo, X.B.; Luo, Q.S.; Liu, X.J.; Chen, X.; Jiang, Z.X. Diagenetic evolution and formation mechanism of dissolved pore of shale oil reservoirs of Lucaogou formation in Malang sag. *J. China Univ. Pet.* **2012**, *36*, 38–43+53.

52. Boles, J.R.; Franks, S.G. Clay Diagenesis in Wilcox Sandstones of Southwest Texas: Implications of Smectite Diagenesis on Sandstone Cementation. *J. Sedmentary Petrol.* **1979**, *49*, 55–70.

53. Peltonen, C.; Marcussen, Ø.; Bjørlykke, K.; Jahren, J. Clay Mineral Diagenesis and Quartz Cementation in Mudstones: The Effects of Smectite to Illite Reaction on Rock Properties. *Mar. Pet. Geol.* **2009**, *26*, 887–898. [CrossRef]

54. Zhang, P.H.; Chen, Z.Y.; Xue, L.; Bao, Y.J.; Fang, Y. The differential diagenetic evolution and its influencing factors of Lower Cambrian black rock series in the northwestern margin of Tarim Basin. *Acta Petrol. Sin.* **2020**, *36*, 3463–3476.

55. Zhao, J.H.; Jin, Z.J. Mudstone diagenesis: Research advances and prospects. *Acta Sedimentol. Sin.* **2021**, *39*, 58–72. [CrossRef]

56. Bernard, S.; Horsfield, B. Reply to Comment on "Formation of Nanoporous Pyrobitumen Residues during Maturation of the Barnett Shale (Fort Worth Basin). *Int. J. Coal Geol.* **2014**, *127*, 114–115. [CrossRef]

57. Liu, B.; Mastalerz, M.; Schieber, J. SEM Petrography of Dispersed Organic Matter in Black Shales: A Review. *Earth-Sci. Rev.* **2022**, *224*, 103874. [CrossRef]

58. Song, D.J.; Tuo, J.C.; Wang, Y.T.; Wu, C.J.; Zhang, M.F. Research advances on characteristics of nanopore structure of organic-rich shales. *Acta Sedimentol. Sin.* **2019**, *37*, 1309–1324. [CrossRef]